SUPPLEMENTARY METHODS

Qubit Fabrication

The first four sets of qubits were fabricated on 550 μm thick c-plane sapphire wafers (double-side polished, HEMEX grade HEM Sapphire) at the Pritzker Nanofabrication (PNF) facility. These wafers were first solvent cleaned by sonicating in n-methyl-2-pyrrolidone (NMP) heated to 80°C followed by sequential soaks in isopropanol, acetone, isopropanol, and deionized (DI) water under mild sonication at room temperature. The sapphire wafers were subject to further cleaning in a mixture of DI water, 30% ammonium hydroxide in water, 30% hydrogen peroxide in water with a 5:1:1 ratio. This cleaning was performed at 65°C for 5 minutes followed by DI water rinse. Following the surface treatments, the substrate was immediately placed inside an AJA ATC 2200 sputtering system with a base pressure less than 10^{-7} Torr. After dehydrating the substrate under vacuum at 200°C for 30 minutes, the wafers were allowed to cool-down before Nb was sputtered at room temperature. DC magnetron sputtering was performed using a 3-inch diameter Nb target with a metals basis purity of 99.95% with an Ar flow rate of 30 sccm and partial pressure of 3.5 mTorr. A sputtering power of 600 W was used and the substrate was rotated at 20 rpm. These conditions resulted in a deposition rate of approximately 19 nm/min. For the qubits prepared on silicon substrates the process involved first cleaning the substrate with a RCA surface treatment detailed previously [1] followed by a buffered oxide etch, before immediately loading into the sputter deposition system [2]. In this case, Nb films were deposited by high power impulse magnetron sputtering with a 6-inch diameter Nb target having a metal basis purity of 99.9995% with a base pressure less than 1E-8 Torr at room temperature.

For the Nb samples capped with Ta or Al, the capping layers were immediately sputtered onto the Nb film *in situ*, i.e. without breaking vacuum in the deposition chamber. Al was deposited from a 3-inch diameter Al target (metals basis purity of 99.9995%) with a DC sputtering power of 500 W. Ta was deposited from a 3-inch diameter Ta target (metals basis purity of 99.95%) with an RF sputtering power of 600 W. The flow rate and substrate rotation speed were kept constant. The Ar partial pressure was increased to 5 mTorr for the Ta encapsulation layer.

For the Nb films capped with TiN, the sample was removed from the sputter deposition system and immediately loaded into an Ultratech/Cambridge Fiji G2 Plasma-Enhanced ALD system for atomic layer deposition of TiN. The TiN ALD recipe comprised of a 250 ms TDMAT, ($Ti(N(CH_3)_2)_4$) precursor dose and a 30 s N_2 plasma exposure. Each of these pulses was separated by a 5 s purge. This process was repeated for 40 cycles and the sample was held at 270°C during the course of this deposition. These capped layers were all between 10-15 nm in thickness.

For the Nb films capped with Au, the sample was removed from the sputter deposition system and immediately loaded into an Angstrom EvoVac Electron Beam Evaporator system with a base pressure of 2E-7 Torr. The Nb surface oxide was milled away with Ar^+ ions for 15 min with a beam voltage of 400 V, an accelerator voltage of 80 V and an ion current of 15 mA. A 10 nm layer of Au was subsequently deposited using e-beam deposition at a rate of 1 angstrom/second. During this process, the substrate was rotated at 10 rpm.

Following film deposition, the superconducting microwave circuit was patterned with photolithography using a Heidelberg MLA 150 Advanced Maskless Aligner. After exposure and development of the photoresist, the circuit layer was defined by dry etching using an inductively coupled plasma - reactive ion etching (ICP-RIE) system. Dry etching was performed using a mixture of Cl_2:BCl_3:Ar with flow rates 30:10:10 sccm. The etching process was halted following the etching of the Nb metal as well as some of the underlying substrate. In the case of sapphire, the substrate was overetched by 20nm and in the case of silicon, the substrate was overetched by 70nm. The remaining photoresist was stripped from the patterned substrate first by ashing in O_2 (to remove the hardened photoresist on the surface) and then by soaking in NMP heated to 80°C for several hours.

The Dolan bridge style Al/AlOx/Al Josephson junctions are fabricated using the well-known double angle shadow evaporation technique and solvent lift off for the samples prepared on sapphire [3]. The junction patterns are exposed using an electron beam with an accelerating voltage of 100kV. The JJ layers for the samples prepared on silicon are deposited using a double-angle bridge-less lift-off lithography process. In a subsequent lithography and metal lift-off step, galvanic connection between the Josephson junctions and the microwave circuitry is established. Ar ion milling is employed to remove surface oxides immediately prior to Al deposition. Following lift-off of the junction leads, the surface is exposed to a mild UV ozone treatment for 10 min to remove residual resist.

The geometry of the qubit consists of a pair of rectangular shunting capacitor paddles joined by a single Josephson junction as seen in Fig. 1a. The paddle size, hence the capacitance, is varied while the gap is kept fixed. A geometry similar to this has exhibited greater than 300 μs qubit coherence times in the past[4]. To minimize the influence of the magnetic flux noise, all qubits are designed to have fixed frequencies. Following the circuit quantum electrodynamics (cQED) architecture [5], each qubit is capacitively coupled to a single quarter-wave readout resonator. Each of these resonators is inductively coupled to a 50 Ω transmission line where a microwave probe tone can be sent to the resonator. On a single 7.5×7.5 mm^2 sapphire chip, there are four qubits with this rectangular-paddle geometry. The resonator frequencies are evenly spaced between 6.8 and 7.2 GHz with qubit frequencies ranging from 3.4-6 GHz as summarized in Supplementary Tables 1 and 2.

Qubit Measurement Setup and Method

Each qubit chip was packaged in a gold plated copper box, where it is mounted on a cold finger directly attached to the dilution refrigerator (DR) mixing plate. Both the enclosure and the cold finger are made of gold-coated copper to reduce thermal resistance between the qubit chip and the enclosure. Each qubit chip is protected from IR photons with Eccosorb filters on both input and output lines. All qubit enclosures and Eccosorb filters are enclosed within magnetic shielding to reduce flux noise and are wired to cryogenic switches anchored on the mixing stage. This way, all qubits share the same microwave input and output lines, which enables comparison of different qubits. A total of 52 dB attenuation is distributed across different temperature stages to effectively suppress thermal noise below 10^{-3} noise photon number [6]. Three cryogenic isolators with a total of 60 dB isolation at the output line reduces the backaction noise arising from the high electron mobility transistor (HEMT) amplifier mounted on the 3K stage. Low-pass filters (K&L Microwave) are used to remove the high-frequency noise above 10 GHz.

The qubit state is measured via dispersive readout, in which the qubit frequency is far detuned from the resonator frequency ($\Delta = f_q - f_r$) so that $\Delta \gg \kappa, g$, where κ and g are the resonator linewidth and qubit-resonator coupling strengths, respectively [7]. In this case, the qubit and resonator do not directly exchange energy. Instead, the qubit induces a state-dependent frequency shift of the resonator. By interrogating the resonator, the qubit state can be inferred.

Qubit measurements of devices on Si substrates were performed in a different dilution refrigerator with a similar configuration. Chips were attached to a thermally anchored printed circuit board on the mixing chamber plate of a dilution refrigerator with a base temperature of 10 mK. The devices are shielded from magnetic fields with superconducting and cryoperm cans with a blackbody absorber to suppress stray infrared radiation. The input signal chain has a total attenuation of 76 dB achieved by a series of attenuators anchored at different temperatures, and a 7.65 GHz low-pass filter. The output signal line is filtered by isolators and amplified by a HEMT at 4K and a series of room-temperature amplifiers. Relaxation times are measured in the dispersive regime continuously on each device over multiple days.

TEM Sample Preparation

TEM samples were prepared using a 30 kV focused Ga^+ ion beam. In order to protect the surface oxide during the ion milling process, the sample was first coated with 50 nm of carbon. The samples were finely polished to a thickness of roughly 50 nm using 5 kV and 2 kV Ga^+ ions in an effort to remove surface damage and amorphization in the regions of interest.

STEM Data Collection

EDS data was acquired using a JEOL ARM 200CF ARM S/TEM operated at 200 kV. The camera length is set to 8 cm and the condenser aperture is selected to provide a convergence semi-angle of 30 mrad with beam current $\sim$ 20 pA in order to minimize beam-induced damage. The intensity of the Nb Lα and Ta Lα signals were plotted as a function of position for the Ta-capped Nb sample. The intensity of the Nb Lα and Al Kα signals were plotted as a function of position for the Al-capped Nb sample. The intensity of the Nb Lα, Ti Kα, and N Kα signals were plotted as a function of position for the TiN-capped Nb sample. The intensity of the Nb Kα and Au Lα signals were plotted as a function of position for the Au-capped Nb sample. In order to prepare the chemical maps presented in Fig. 2a-c, the individual chemical maps for each sample were normalized, overlaid, and low-pass filtered using a Gaussian function with $\sigma = 2$. The EELS data and associated HAADF STEM image was acquired using a Titan Themis with GIF quantum ER system. Electron diffraction patterns from the Ta oxide was collected on JEOL 300F Grand ARM S/TEM using an accelerating voltage of 300kV. In this case, the camera length is set to 20 cm and the condenser aperture is selected to provide a convergence semi-angle of 1 mrad. Four-dimensional STEM (4D-STEM) data sets [8] were acquired in a 200 x 100 mesh (with pixel size of 1.6 nm) across the thin films using a Gatan OneView camera and synchronized using STEMx.

SUPPLEMENTARY TABLES

Qubit T1 Measurements

Geometry	**Film**	**Qubit Frequency** (MHz)	**Average T1** (μs)	**Q** (millions)
A	Nb	5986	54	2.0
A	Nb	5796	21	0.8
A	Nb/TiN	4990	60	1.9
A	Nb/TiN	4721	105	3.1
A	Nb/TiN	4645	55	1.6
A	Nb/Al	4894	77	2.4
A	Nb/Al	4968	69	2.2
A	Nb/Al	4586	86	2.5
A	Nb/Al	4512	78	2.2
A	Nb/Au	4637	80	2.3
A	Nb/Au	4077	134	3.4
A	Nb/Au	4185	100	2.6
A	Nb/Au	4193	120	3.2
A	Nb/Au	4657	109	3.2
A	Nb/Au	4749	137	4.1
A	Nb/Au	4782	27	0.8
A	Nb/Ta	5005	102	3.2
A	Nb/Ta	4746	118	3.5
A	Nb/Ta	4707	103	3.0
A	Nb/Ta	4488	161	4.5

Supplementary Table 1: Summary of qubit devices prepared with different capping layers.

Geometry	**Film**	**Qubit Frequency** (MHz)	**Average T1** (μs)	**Q** (millions)
A	Nb/Ta	3476	131	2.9
A	Nb/Ta	3485	136	3.0
A	Nb/Ta	3477	186	4.1
A	Nb/Ta	3530	120	2.7
B	Nb/Ta	3945	280	6.9
B	Nb/Ta	3952	324	8.0
B	Nb/Ta	3814	262	6.3
B	Nb/Ta	3930	214	5.3
C	Nb/Ta	3737	193	4.5
C	Nb/Ta	3634	199	4.5
C	Nb/Ta	3904	109	2.7

Supplementary Table 2: Summary of Nb/Ta qubit devices with different geometries.

SUPPLEMENTARY FIGURES

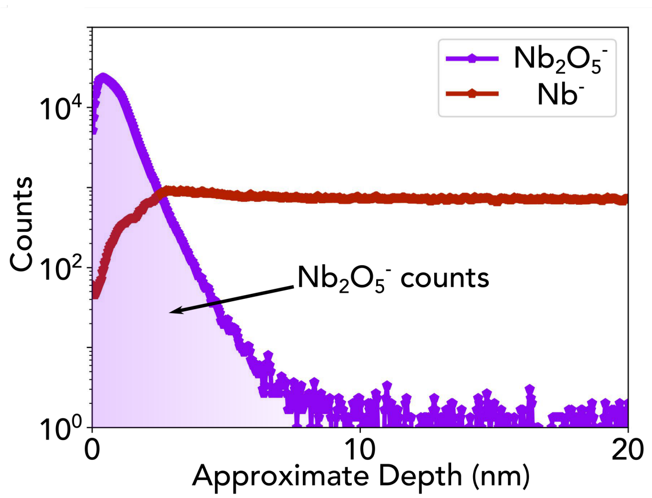

Supplementary Figure 1: ToF-SIMS Depth profile taken from the surface of Nb film. The Nb_2O_5 region is labeled. Fig. 2e is constructed by taking the integrated counts of the $Nb_2O_5^-$ for each of the samples using the same ion beam conditions.

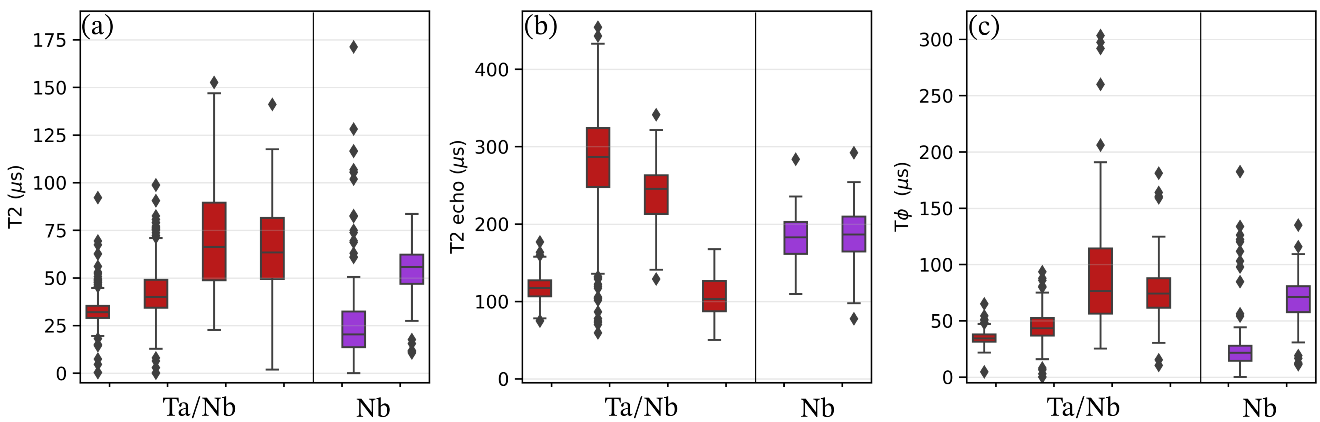

Supplementary Figure 2: Box plot displaying measured (a) T_2, (b) $T_{2\,\mathrm{echo}}$, and (c) T_ϕ values for test devices fabricated on silicon substrates. Boxes mark the 25th percentile and the 75th percentile of the measurement distribution. The line inside each box represents the median value. Error bars represent 95% confidence interval and circles represent outliers. The T_2, $T_{2\,\mathrm{echo}}$, and T_ϕ values also increase following capping of Nb with Ta, although the spread in values is larger, as expected given their dependencies on additional extrinsic factors.

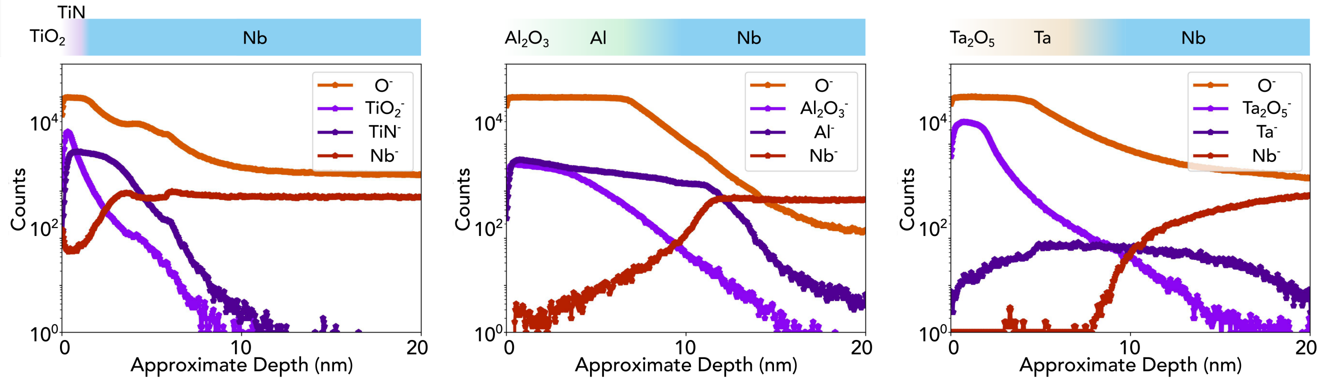

Supplementary Figure 3: ToF-SIMS depth profiles taken from the surface of Nb films capped with TiN, Al, and Ta. TiO_2, Al_2O_3, and Ta_2O_5, respectively are observed at the surface of these films.

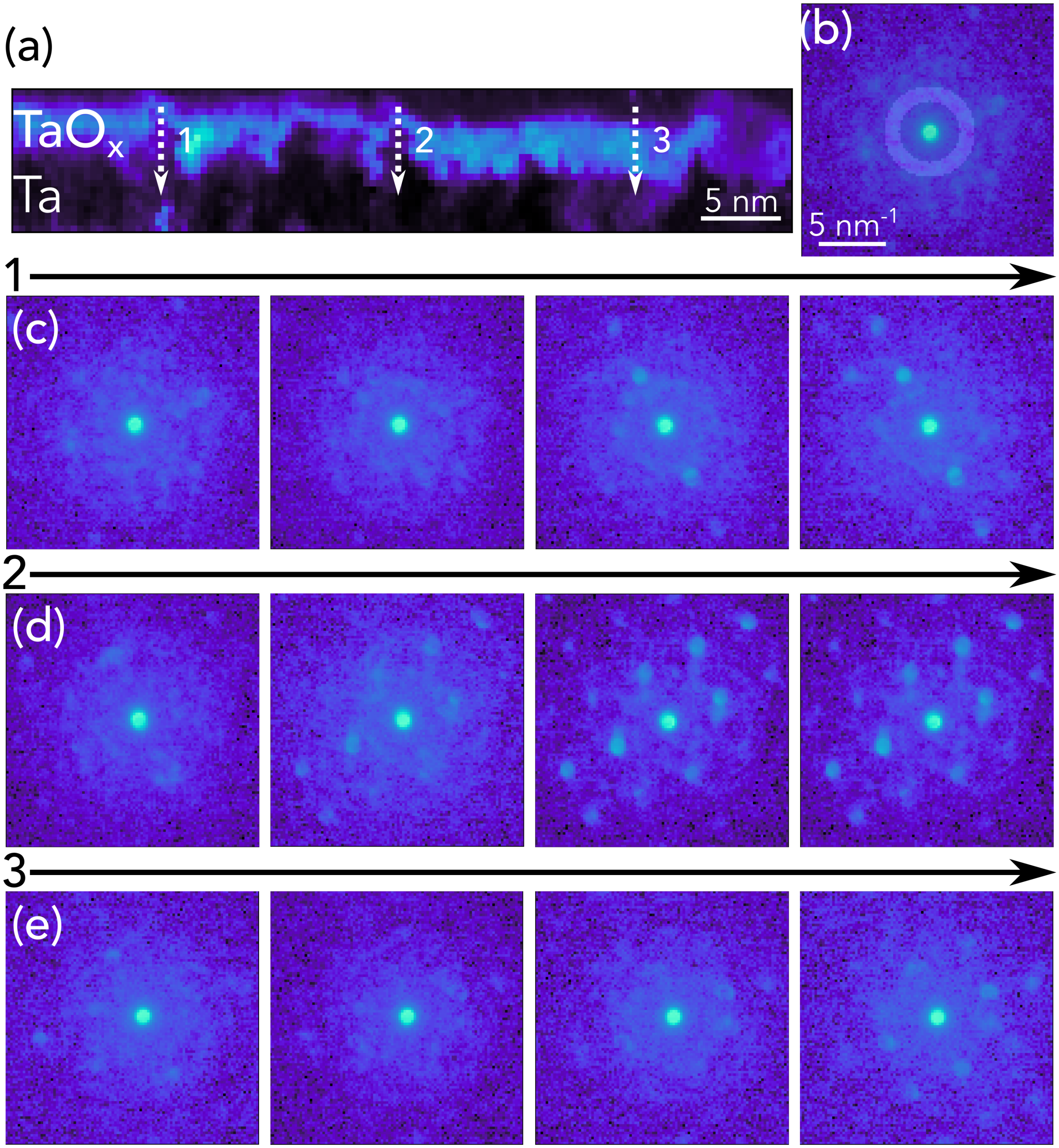

Supplementary Figure 4: (a) DF image of Ta oxide/Ta interface using a virtual detector that matches the diffraction ring of the Ta oxide. The dotted arrows indicate regions over which changes in the diffraction pattern are provided in (c-e). (b) Diffraction pattern taken from TaO_x with a virtual annular detector. The radius of the inner ring is 2.07 nm^{-1} and the radius of the outer ring is 3.25 nm^{-1} in order to preferentially produce a TaO_x dark field image. (c-f) Changes in the electron diffraction pattern in the direction of the arrows indicated in (a) for the labeled regions 1, 2, 3, and 4, respectively. In all cases, a diffuse diffraction pattern, which is characteristic of an amorphous solid is observed for the TaO_x. Intense diffraction spots tend to appear when moving towards the crystalline Ta metal.

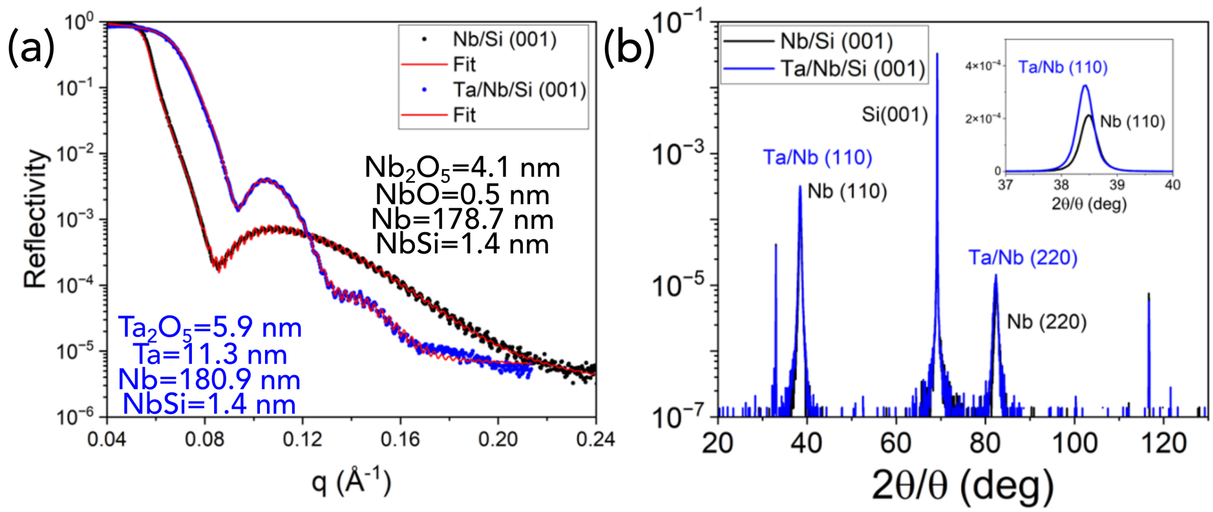

Supplementary Figure 5: X-ray reflectivity (a) and x-ray diffraction (b) pattern taken from both the Nb sample and the Nb sample capped with Ta. Fits based on dynamical scattering suggests that the surface oxide of Nb consists of roughly 4.1 nm of Nb_2O_5 and 0.5 nm of NbO whereas the surface oxide of Ta consists entirely of 5.9 nm of Ta_2O_5. X-ray diffraction pattern suggest both sets of films exhibit the body-centered cubic (BCC) crystal structure and predominantly exhibit {110} texture. For Ta, this crystal structure is associated with the α phase.

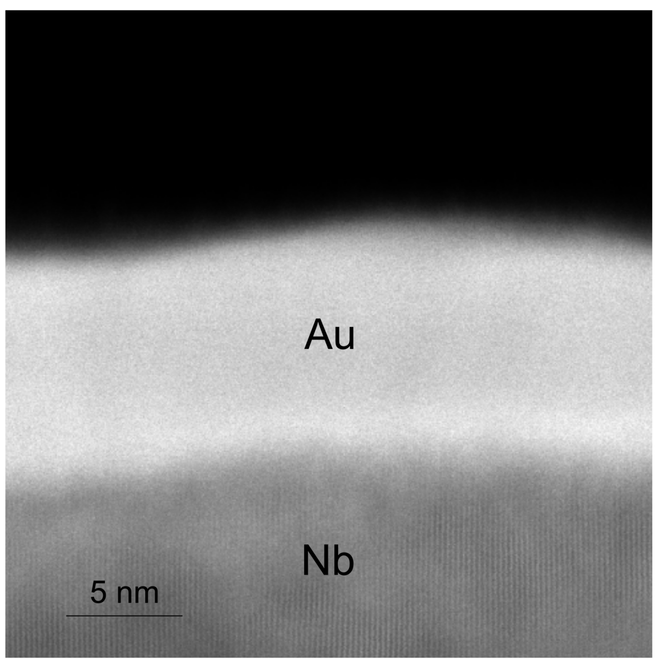

Supplementary Figure 6: High resolution scanning transmission electron microscopy image taken from the Nb film capped with Au. In this case, no oxide is observed at the surface.